Sādhanā (2018) 43:184
https://doi.org/10.1007/s12046-018-0954-3

Thermal performance prediction models for a pulsating heat pipe using Artificial Neural Network (ANN) and Regression/Correlation Analysis (RCA)

VIPUL M PATEL and HEMANTKUMAR B MEHTA*

Department of Mechanical Engineering, Sardar Vallabhbhai National Institute of Technology, Surat 395007, India
e-mail: patelvipulm1992@gmail.com; hbm@med.svnit.ac.in; hemantbmehta@gmail.com

MS received 25 September 2017; revised 18 May 2018; accepted 30 May 2018; published online 5 October 2018

Abstract. Pulsating heat pipe (PHP) is one of the prominent research areas in the family of heat pipes. Heat transfer and fluid flow mechanism associated with PHP are quite involved. The analytical models are simple in nature and limited in scope and applicability. The regression models and Artificial Neural Network (ANN) are also limited to a number of input parameters, their ranges and accuracy. The present paper discusses the thermal performance prediction models of a PHP based on ANN and RCA approach. Totally 1652 experimental data are collected from the literature (2003–2017). Nine major influencing input variables are considered for the first time to develop the prediction models. Feed-forward back-propagation neural network is developed and verified. Backward regression analysis is used in RCA-based regression model. Linear and power-law regression correlations are developed for input heat flux in terms of dimensionless Kutateladze (*Ku*) number, which is a function of Jakob number (*Ja*), Morton number (*Mo*), Bond number (*Bo*), Prandtl number (*Pr*) and geometry of a PHP. The prediction accuracy of present regression models (R^2 = 0.95) is observed to be better as compared with literature-based correlations.

Keywords. PHP; prediction models; ANN; RCA; Kutateladze (*Ku*) number.

1. Introduction

Pulsating heat pipe (PHP) is a two-phase heat removal device that works on the phase change phenomena. It has become a promising passive cooling technique after its invention by Akachi [1] in the field of electronics, space, manufacturing and automobile due to wickless structure, same directional liquid–vapour flow and shape flexibility compared with the heat pipe. It consists of three sections, namely an evaporator section, an adiabatic section and a condenser section (figure 1). In PHP, heat is received from the source via evaporator section and rejected through the condenser section. The adiabatic section can be added to or removed from a PHP based on the application. Heat is transmitted from the evaporator to the condenser by the oscillating/pulsating motion of two-phase vapour bubble and liquid slug [2].

PHP has been investigated by several researchers since its invention in 1990. Experimental investigations carried out on a PHP during 2009–2016 are reviewed by Han *et al* [3]. They reported geometrical parameters, operational parameters and working fluids (WFs) as influencing parameters to predict the thermal performance of a PHP. They grouped inner diameter (D_i) and number of turns (N) as geometrical parameters, and filling ratio (FR), orientation of a PHP (θ) and heat flux (q) as operational parameters. Pure fluids, binary fluids and nanofluids are considered as WFs. Alongside this review, the authors have also performed the experimental investigations on a PHP with various WFs [4] and observed that these parameters influence the internal heat and mass transfer mechanism significantly and make a PHP more complex.

In conjunction with the experimental investigations on a PHP, theoretical prediction models are proposed to understand the complex thermo-hydrodynamics of a PHP. As heat transfer from evaporator to condenser in a PHP is mainly due to the oscillating/pulsating motion of vapour bubbles and liquid slugs, various models are developed to understand the influence of oscillating/pulsating motions on heat transfer [5–9]. In order to predict the thermal performance of a PHP, heat transfer correlations are developed [10–13]. However, these correlations were developed with limited experimental data and applicable at specified operational ranges. Chaotic behaviour of a PHP is analysed based on wall temperature fluctuations and implementing various nonlinear models [14, 15]. Start-up mechanism and start-up heat flux correlation of a PHP are theoretically reported by Qu and Ma [16]. Numerical

*For correspondence

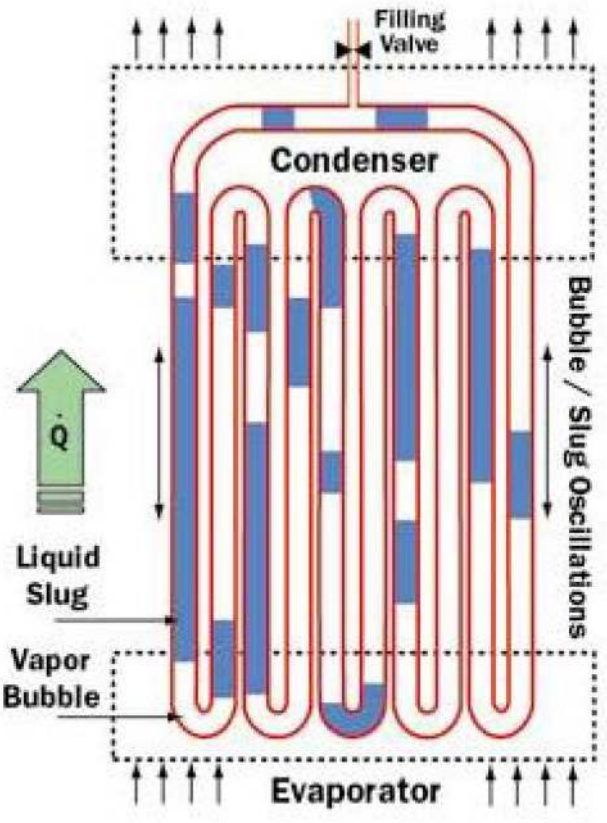

Figure 1. Pulsating heat pipe [2].

investigations are carried out with limited mass transfer mechanism and dimensionality of the PHP [17, 18]. Artificial Neural Network (ANN) methods are also reported to predict the nonlinear behaviour and thermal performance of a PHP [19–23]. Nevertheless, it is worth noting that influence of flow pattern transition during operation on the oscillating/pulsating motion of vapour bubbles and liquid slugs is not considered. Moreover, prediction models are developed with a limited number of vapour bubbles, liquid slugs and input parameters. It is therefore difficult to develop a prediction model of a PHP involving intricate heat and mass transfer mechanism due to simplified physics and limited influencing parameters. There is no unified heat transfer correlation available that can effectively predict the thermal performance of a PHP. Hence, the development of a unified heat transfer correlation involving all major influencing parameters for a PHP is still challenging due to diverse experimental dataset reported in the literature. In view of these facts, the present research work is carried out to develop thermal performance prediction models of a PHP using ANN and RCA approach.

2. Data collection

Thermal performance of a PHP is a function of geometrical parameters (D_i, D_o, L_e, L_c, N), working fluids (WFs) and operational parameters (θ, FR, Q). In order to systematically investigate the models and to develop unified heat transfer correlation, totally 1652 experimental data of copper-based closed loop PHP are collected from the available literature (2003–2016) and tabulated in table 1. Water, methanol, ethanol, acetone, R-123 and FC-72 are considered as WFs and numbered in order as 1–6 in the table. Three orientations of a PHP reported in the literature are considered for modelling specified as vertical bottom heating ($\theta = 0°$), horizontal heating ($\theta = 90°$) and top heating ($\theta = 180°$). The range of each parameter is separately shown in table 2.

In order to estimate the prediction accuracy of models developed using ANN and RCA, the experimental data reported by authors [4] are used. Various WFs considered in the experiments are deionized (DI) water (1), methanol (2), ethanol (3) and acetone (4) as pure fluids, $FR = 50\%$, $D_i = 2$ mm, $D_o = 4$ mm, $L_e = 40$ mm, $L_c = 50$ mm, $N = 9$ and $Q = 10$–110 W. Thermal resistance (R_{th}) was considered as a performance parameter of a PHP. As shown in figure 2, R_{th} is observed to decrease (1.43–0.34 K/W) with an increase in heat input (10–110 W) and found to be the minimum for acetone as compared with its counterpart fluids.

3. Thermal performance prediction models

This section discusses the construction and comparison of prediction models developed based on a wide range of 1652 experimental data using ANN and Regression/Correlation Analysis (RCA). These models are developed with totally nine input parameters such as inner diameter (D_i), outer diameter (D_o), evaporator length (L_e), condenser length (L_c), number of turns (N), working fluids (WFs), orientation (θ), FR and heat input (Q). Thermal resistance (R_{th}) is considered as an output parameter. Each prediction model is systematically discussed in the subsequent sections.

3.1 *Prediction model using ANN*

ANN is a data-driven machine learning tool to mimic the human brain and nervous system. It consists of large interconnected processing elements called neurons. It has an input layer (receives data), a hidden layer (processes data) and an output layer (sends computed information). These layers can learn, memorize and establish a relationship between inputs and outputs and make ANN better than an empirical model [49]. The desired output is obtained by adjusting associated weights through a learning process to match with actual output.

In recent years, ANN has proved its capability to effectively predict the behaviour of a complex and nonlinear system [50, 51]. ANN modelling of a PHP is reported by various researchers as tabulated in table 3. However, these ANN models are limited to a number of input parameters

Table 1. Experimental dataset of various researchers.

Researchers	D_i (mm)	D_o (mm)	L_e (mm)	L_c (mm)	N	WF	FR	θ	Q (W)	R_{th} (K/W)
Chien *et al* [24]	2	–	15	40	8	1	40–70	0–90	10–130	0.62–2.13
Karthikeyan *et al* [25]	2.3	3.3	40	60	5	1	50	0	50–180	0.65–0.73
Lin *et al* [26]	2.4	3	22	35	5	1	20–80	0	9–87	0.83–2.88
Baitule [27]	2	3	360	280	2	1,2,3,4	0–100	0	7–81	0.28–3.48
Clement and Wang [28]	1.6	3.1	156	156	8	3	45	0	100–150	0.22–1.15
Shafii *et al* [29]	1.8	3	60	60	5	1,2	30–80	0	5–70	1.06–4.69
Verma *et al* [30]	1.45	2.54	40	30	6	1,3	10–100	0–90	10–100	0.5–2.49
Naik *et al* [31]	1.95	3	185	195	1	4	60,70,80	90	9–15	1.72–3.24
Tseng *et al* [32]	2.4	3	70	70	4	3	60	90	10–140	0.94–2.82
Ji *et al* [33]	1.65	3.18	40	64	6	1	50–76	0	15–200	0.16–2.64
Kothare *et al* [34]	1.5, 2	2.9,3.6	60	80	4	2	50	0	10–130	0.67–1.85
Pachghare and Mahalle [35]	2	3.6	42	50	2	1,2,3,4	50	0	7–80	0.27–4.71
Han *et al* [36]	2	4	80	80	5	1,2,3,4	35,45	0	10–50	0.27–1.74
Wang *et al* [37]	1.3	2.5	35	35	4	1	50	0,90	10–80	0.89–2.02
Mohammadi *et al* [38]	2.2	3.2	82	53	4	1	25–70	0–90	25–85	0.5–3.42
Wang *et al* [39]	2	4	24	106	5	2,4	35–70	0	25–125	0.17–1.95
Mameli *et al* [40]	2	4	80	80	5	1,3,4	35–70	0	5–100	0.11–2.04
Cui *et al* [41]	2	4	80	80	5	1,2,3,4	20–95	0	5–100	0.09–2.46
Pachghare and Mahalle [42]	2	3.6	50	50	10	1,2,3,4	50	0	10–100	0.34–1
Borkar *et al* [43]	2	3.6	42	50	1,2,3	1,2,3,4	30–70	0	7–80	0.17–2.76
Yang *et al* [44]	1,2	2,3	8	120	20	5	30,50,70	0–180	20–533	0.31–0.65
Khandekar *et al* [45]	2	3	30	120	5	1,2	0–100	0	4–70	1.18–3.71
Akter Jahan *et al* [46]	2	3	395	315	5	1,2	70	0–90	4–73	0.55–8.65
Han *et al* [47]	2	4	80	80	5	1,2,3,4	20–95	0	5–100	0.10–2.17
Mameli *et al* [48]	1.1	2	6	180	16	6	50	0–90	10–100	0.28–1.56

Table 2. Range of parameters used for modelling.

Parameters	D_i (mm)	D_o (mm)	L_e (mm)	L_c (mm)	N	WF	FR	Θ	Q (W)	R_{th} (K/W)
Range	1–2.4	2–4	6–395	30–315	1–20	1–6	0–100	0–180	4.07–532.78	0.11–8.65

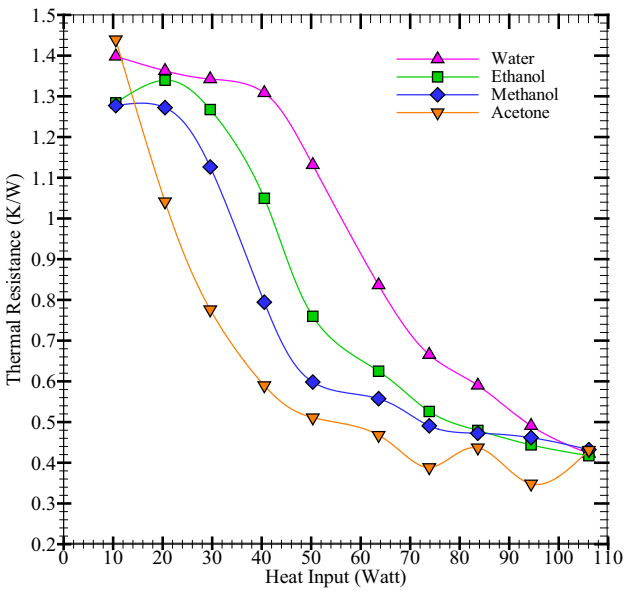

Figure 2. Thermal resistance versus heating power input for different pure fluids [4].

and experimental data considered for the modelling of a PHP. Since the working of a PHP is intricate in nature, a limited number of input parameters and experimental data cannot predict the performance of a PHP accurately. Hence, the present ANN modelling involves nine major influencing input parameters and a wide range of 1652 experimental data.

The present ANN model is developed using a neural network toolbox of MATLAB. The feed-forward network based on the back-propagation learning procedure is used to develop the present ANN model. Totally nine geometrical and operational parameters are considered as input variables and thermal resistance (R_{th}) of a PHP is set as an output parameter. Neurons of input layer receive the information from nine input variables. The input layer passes these data to the first hidden layer. The weighted input parameters (weight × input parameter) and bias are processed through a transfer function in this layer. Sigmoidal (tansig) function (Eq. (1)) is extensively used as a transfer function [52–55]. The preliminary output of the first hidden layer goes to the second hidden layer. The process is repeated in the second hidden layer and generates

Table 3. ANN modelling of a PHP.

Researchers	Input parameters	Output parameter	ANN	Data
[19]	Heat input Filling ratio Inclination angle	R_{th}	Feedforward multi-layer neural network with back propagation Layer = 2 Neuron = 40–50	240
[20]	Heat input Filling ratio	R_{th}	Feedforward multi-layer neural network with back propagation Layer = 3 Neuron < 10	76
[21]	Working fluid Filling ratio Heat input	R_{th}	2-layer neural network with back propagation Layer = 2	–
[22]	Heat input Filling ratio	R_{th}	Using different possible neural models by a combination of various networks and transfer functions Layer = 2 Neuron = 10 Transfer functions: Purelin, logsig, tansig and Gaussian RBF	47
[23]	Filling ratio Inclination angle Heat input	Q	Functional chain neural network	–

the final output in the output layer (R_{th}). This signal flow from input to output in a network is unidirectional and hence known as feed-forward network. The output layer compares output data with original targeted data and generates an error. Weights and bias of each neuron in hidden layers are updated based on the Mean Square Error (MSE) as per Eq. (2) and this process is continued in order to obtain the acceptable MSE. This is achieved using back-propagation learning procedure during data training that works with the supervised learning method. The Levenberg–Marquardt optimization algorithm is universally adopted in training process due to its significant advantages of high speed, capability and robustness [52–56].

$$\tan sig(x) = \frac{2}{1+e^{-2x}} - 1, \quad (1)$$

$$\text{MSE} = \frac{1}{n}\sum_{i=1}^{n}(\text{target value}_i - \text{predicted value}_i)^2. \quad (2)$$

ANN is a data-driven model and hence requires a large number of data to accurately predict the output. Out of totally 1652 data, 53 data are arbitrarily selected for confirmation and verification of final ANN model. Remaining 1599 experimental data are used to develop the ANN model. In the development of the ANN model, 1599 data are arbitrarily divided into three parts. The training dataset uses 1119 data (70% data) to adjust the weights during the training process; 240 data (15% data) are used for validation purpose to minimize overfitting of data and remaining 240 data (15% data) are set as testing data.

ANN structure size depends on the data size and type of system. Optimal ANN structure requires a specific number of hidden layers with an optimal number of neurons. An ANN structure with a minimum of two hidden layers and optimal neurons is able to model the complex behaviour of PHP system [19–22]. ANN model with an excessive number of neurons causes overfitting, additional unnecessary training time and leads to complex interconnection weight structure whereas an inadequate number of neurons are not able to learn the complete relationship between data. Evaluation of an optimal number of neurons is achieved through trial and error based on the criteria of R (coefficient of correlation). Totally 11 ANN models are developed based on the number of neurons (10–20) and tabulated in table 4. The value of overall R is found to be the maximum (0.9448) for the fifth ANN model with 14 number of neurons. Hence, the optimal ANN model is framed as input layer with nine input variables (i = 1, 2, …, 9), first hidden layers with 14 neurons (j = 1, 2, 3, …, 14), second hidden layer with one neuron (H_2) and an output layer with output parameter (R_{th}). Evaluation of R_{th} is carried out using Eqs. (3)–(6) and associated weights and

Table 4. Various ANN models based on number of neurons.

ANN models	Number of neurons	R			
		Training	Validation	Testing	Overall
1	10	0.9183	0.9138	0.8477	0.9054
2	11	0.9079	0.8747	0.9012	0.9022
3	12	0.8973	0.8782	0.9021	0.8954
4	13	0.9333	0.9215	0.8900	0.9256
5	14	0.9405	0.9561	0.9539	0.9447
6	15	0.9251	0.8921	0.9191	0.9173
7	16	0.9378	0.9193	0.9036	0.9292
8	17	0.9552	0.9099	0.9236	0.9428
9	18	0.9100	0.8802	0.9074	0.9051
10	19	0.9530	0.9262	0.7812	0.9164
11	20	0.9557	0.9353	0.8885	0.9379

Table 5. Associated weights and bias of the first hidden layer of an optimal ANN model.

	Input variables (i)									
Number of neurons (j)	D_i	D_o	L_e	L_c	N	WF	θ	FR	Q	Bias (b)
1	−3.2929	−0.1933	0.6644	1.5046	0.4403	−0.0708	−1.2960	1.5618	0.1680	3.1185
2	−0.6471	0.4798	0.2466	0.0912	0.1536	−0.0823	−0.1365	−8.6131	0.0882	−9.4070
3	1.2712	−1.0313	0.0382	0.5366	1.5161	−0.4450	−0.3597	−2.6603	2.7851	1.5535
4	−2.5552	−1.1144	0.5360	−1.0508	−2.1014	−0.9898	−1.1787	−3.1578	0.1680	0.8617
5	−0.2048	0.6906	0.2940	−0.8724	−0.4717	0.3748	−2.3945	3.5125	−2.7860	−2.2907
6	0.9731	−0.4258	−3.1084	−2.8252	−1.9464	−0.2051	−4.3702	0.0332	−2.8879	2.7518
7	−4.4496	−4.5608	3.9540	1.6346	5.0125	−0.9048	−5.0805	3.7491	−0.2409	−1.4578
8	−1.6666	0.0191	−1.4214	2.3920	1.8213	1.0250	−0.0115	1.1216	−0.1236	1.2238
9	−4.1632	−2.7859	0.9291	−1.6471	−1.7167	−0.6125	0.4292	−5.9827	−0.3659	−2.9582
10	−0.3547	−1.0247	−3.0310	−0.0195	1.2400	2.5862	−6.4969	−1.9747	−2.6662	2.6495
11	−1.1480	−1.8113	−3.4641	0.9845	0.8690	3.9924	−4.3079	−1.4587	0.7226	1.7478
12	−1.6138	2.1428	−1.8165	−1.6643	0.7241	−0.1105	2.3250	−2.7649	1.0106	0.7801
13	2.5490	2.7925	1.5785	−2.8404	1.3971	0.5187	0.0058	5.4993	−0.0407	2.6955
14	3.0504	2.8828	0.2016	−6.1782	−0.2471	−3.2247	4.6283	−0.3467	−0.5289	3.3963

Table 6. Associated weights and bias of the second hidden layer of an optimal ANN model.

Neuron	1	2	3	4	5	6	7
Weights	−0.5831	2.6641	5.1166	−2.4253	2.3689	3.9312	−2.6755
Neuron	8	9	10	11	12	13	14
Weights	−2.2685	−0.6420	−4.6273	−3.2372	4.7401	−1.2140	−4.7347
Bias ($bh2$)	0.2805						

biases of each hidden layer of the developed optimal ANN model are tabulated in tables 5 and 6.

Input A (from input layer) to neuron j of the first hidden layer is given by

$$A_j = \sum_{i=1}^{9} x_i w_{ji} + b_j. \tag{3}$$

Output of neuron j of first hidden layer is given by

$$O_j = \frac{2}{1 + e^{-2A_j}} - 1. \tag{4}$$

Input to second hidden layer neuron is given by

$$B = \sum_{j=1}^{14} O_j w_{H2j} + bh2 \tag{5}$$

Output of second hidden layer neuron is given by

$$R_{th} = \frac{2}{1 + e^{-2B}} - 1. \tag{6}$$

The predicted thermal resistance obtained from the present optimal ANN model is compared with the literature-based actual thermal resistance for training dataset as shown in figure 3. Totally 68% predicted data fall within Mean Absolute Relative Deviation (MARD) of 24.12% while remaining 32% data fall outside this range. However,

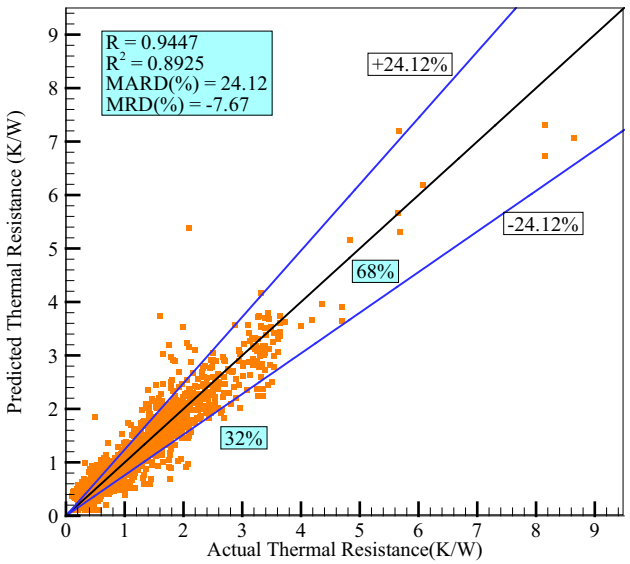

Figure 3. Predicted versus literature-based thermal resistance for training dataset.

the values of R and R^2 are observed to be 0.9447 and 0.8925, respectively, which shows the overall agreement of the predicted dataset with the actual dataset. The prediction accuracy of the developed optimal ANN model is verified with two sets of data: (1) 53 (3.2%) data out of total 1652 literature-based experimental data and (2) 40 data of

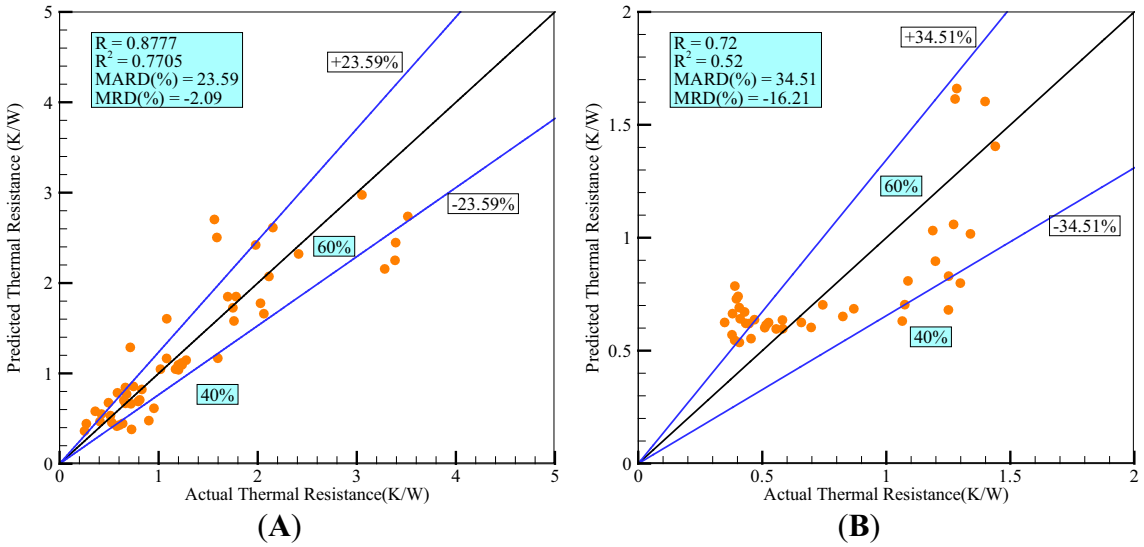

Figure 4. Predicted versus actual thermal resistance for (**a**) literature-based testing dataset and (**b**) authors' experimental dataset [4].

authors' experiments [4] involving four different pure fluids (figure 2); this comparison is shown in figure 4A and B, respectively. As shown in figure 4A, 60% testing data fall within MARD of 23.59% while remaining 40% data fall outside this range. The R and R^2 values are observed as 0.8777 and 0.7705, respectively. This dataset was not used during the development of an optimal ANN and hence it is observed that the present ANN model prediction is consistent with the anonymous dataset. In addition to this, the present ANN predicts thermal resistance with MARD of 34.51% and R=0.72 (R^2 = 0.52) when compared with the authors' dataset [4]. Hence, on involving more input variables with a wide range of dataset, the overall prediction of thermal resistance using ANN is found to be satisfactory with all statistical parameters.

3.2 *Prediction model using RCA*

Statistical analysis is another mathematical tool that can identify trends and correlations within complex datasets. Regression models are statistical methods for estimating the relationship between the output parameter and the input (influencing) parameters. An example of a regression equation is given below:

$$Y_p = A_0 + A_1X_1 + A_2X_2 + \cdots + A_nX_n \tag{7}$$

$$Y = Y_p + e \tag{8}$$

where Y is the real output, Y_p presents the regression model output, X_1–X_n represent the input variables, A_1–A_n represent the coefficients for the corresponding influencing variables, A_0 represents the constant term and e is the associated error term. Usually, the objective of the regression model is to minimize the sum of squared errors by varying the coefficients, A_1–A_n. To measure and compare the performance of the regression models, the following terms are used:

$$\text{Coefficient of Determination } R^2 = 1 - \frac{SSE}{SST} \tag{9}$$

$$\text{Adjusted Coefficient of Determination } R^2_{adj} = 1 - \frac{SSE}{SST} \times \frac{n-1}{n-k-1} \tag{10}$$

In the above equations n represents the number of observations, k is the number of influencing parameters (predictors), Sum Squared Error (SSE) and Sum Squared Total (SST) are the unexplained and total variability of the measured output respectively. R^2 and R^2_{adj} are used to measure the wellness of the fit by the trained models. Regardless of the relationship with the input parameters and output, adding a new parameter to the model results in an increase in R^2. However, R^2_{adj} only increases if the added parameter is actually a proper predictor. Hence, R^2_{adj} is a more useful parameter than R^2 since it is a better indicator of whether introducing a new parameter adds any value to the model. For large datasets, both have similar values since the penalty term $(n-1)/(n-k-1)$ approaches unity when n is large. In addition to this, p-value is used to measure the statistical significance of influencing parameters on the output during backward regression based on t-test. The threshold p-value is considered as 0.05 for the analysis. Null hypothesis (A_1, A_2, …, A_n=0) is investigated based on p-value. Null hypothesis is rejected for p-value less than 0.05 (large t-stat value) and changes in input parameters are significantly related to changes in output. Conversely, if p-value is found to be greater than 0.05 (t-stat close to 0), the parameter will be discarded from the

regression analysis. Backward regression is performed to select the combination of parameters that generate the best model among all parameters. The predictive models are developed for the output parameter. By defining the threshold p-value of 0.05 and performing the backward regression method, all possible predictor parameters are initially considered for developing the model. Subsequently, the least statistically significant parameter with the largest p-value is iteratively removed in a stepwise manner until all the remaining parameters in the model contain a significant predefined p-value < 0.05. This eliminates variables from the model individually. The overall R^2_{adj} is observed every time when a new insignificant variable is removed from the model.

The objective is to build a regression model to predict the thermal performance of a PHP in terms of thermal resistance (R_{th}). R_{th} is modelled as a function of inner diameter (D_i), outer diameter (D_o), evaporator length (L_e), condenser length (L_c), total number of turns (N), working fluids (WFs), orientation (θ), FR and heat input (Q). Total 1652 literature-based experimental data are used to develop the RCA model.

In the present modelling approach, backward regression is performed to select the optimal combination of variables that generates the best prediction model by excluding insignificant variables step by step. The results obtained using backward regression analysis are tabulated in table 7 with all potentially relevant nine input variables. In the first model (model 1), the p-value for all influencing variables except FR and N is less than 0.05. Hence, less-significant variable FR is removed for the next step calculation. In the second step (model 2), N is observed to be less significant compared with other variables and therefore it is removed from the next step iteration. In the third step (model 3), all the variables show significance and hence the calculation stops afterwards. The values of R^2 (0.38) and Adjusted R^2 (0.38) are not observed to be affected by the reduction of input variables. The correlation developed based on the regression analysis is shown as Eq. (11).

$$R_{th} = 1.6983 + 0.8301D_i - 0.4778D_o - 0.0037L_e + 0.0054L_c - 0.2174WF - 0.0041\theta - 0.0062Q. \quad (11)$$

The comparison of the predicted thermal resistance using developed correlation (Eq. (11)) with the literature-based thermal resistance is shown in figure 5. The prediction is not found to be consistent with the actual R_{th}. Moreover, the prediction contribution of the coefficient of an individual parameter is carried out based on the percentage normalizing approach and shown in figure 6. It is observed that the contribution of coefficients of all the variables (except Q) is significant with respect to each other. However, the coefficient value of Q is observed to dominate and govern the entire prediction. This shows that the prediction accuracy of the RCA model depends greatly on the value of Q.

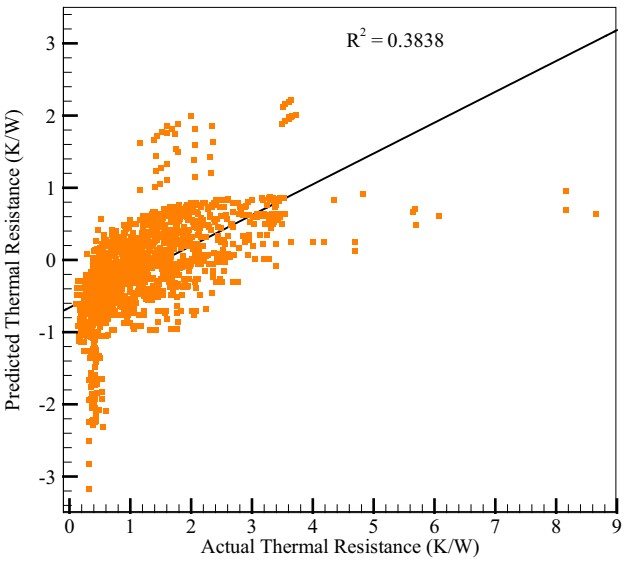

Figure 5. Comparison between predicted (RCA) and literature-based actual thermal resistance.

Table 7. Summary of results obtained using backward regression analysis.

Model no.		Intercept	D_i	D_o	L_e	L_c	WF	θ	Q	N	FR.
01	Coefficients	1.6115	0.8624	−0.4845	−0.0035	0.0052	−0.2190	0.0039	−0.0063	0.0067	**0.0006**
	t-stat	10.2830	8.7411	−9.2764	−8.0795	8.9201	−13.5429	5.8997	−17.4065	0.8393	**0.7269**
	p value	0.0000	0.0000	0.0000	0.0000	0.0000	0.0000	0.0000	0.0000	0.4014	**0.4674**
	R^2 = 0. 0.3843, Adjusted R^2 = 0.3810										
02	Coefficients	1.6353	0.8558	−0.4787	−0.0034	0.0052	−0.2198	0.0039	−0.0063	**0.0071**	*
	t-stat	10.6728	8.7124	−9.2758	−8.0479	8.8934	−13.6199	5.9283	−17.4220	**0.8901**	*
	p value	0.0000	0.0000	0.0000	0.0000	0.0000	0.0000	0.0000	0.0000	**0.3735**	*
	R^2 = 0.3841, Adjusted R^2 = 0.3811										
03	Coefficients	1.6983	0.8301	−0.4778	−0.0037	0.0054	−0.2174	0.0041	−0.0062	*	*
	t-stat	12.5014	8.8437	−9.2611	−10.5705	10.6025	−13.6622	6.9341	−19.6476	*	*
	p value	0.0000	0.0000	0.0000	0.0000	0.0000	0.0000	0.0000	0.0000	*	*
	R^2 = 0.3838, Adjusted R^2 = 0.3812										

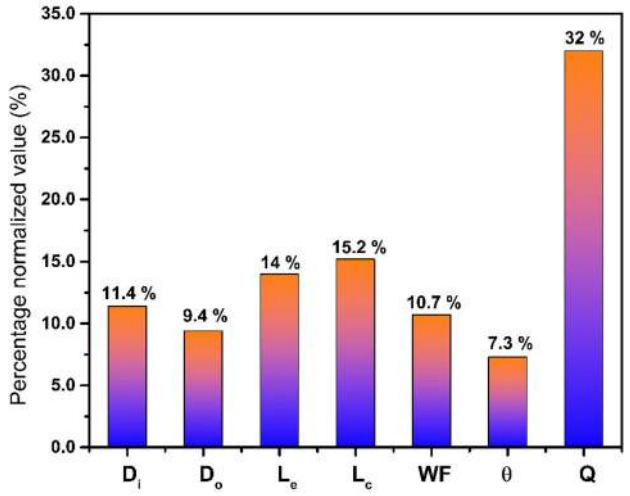

Figure 6. Percentage normalized value of the coefficients of individual parameters.

As discussed earlier, the prediction of thermal resistance using ANN model is reasonably better as compared with RCA model. However, ANN model acts as a black box and does not contribute any significant relationship between input variables and output parameter.

On the contrary, RCA model can develop the input–output relationship but the predicted thermal resistance is not found to be in agreement with the actual R_{th} and heat transfer is observed to dominate for the prediction of thermal resistance. In addition to this, critical heat flux observed is different for different WFs for the same input heat flux. This shows that input heat flux is not reasonable to predict the thermal performance of a PHP. Hence, in the next model development, the thermal performance of a PHP is defined in terms of well-known dimensionless Kutateladze number (Ku), which is defined as the ratio of input heat flux of a PHP to the critical heat flux as per Eq. (12):

$$\text{Kutateladze number } Ku = \frac{q}{h_{lv}\rho_v^{0.5}[\sigma g(\rho_l - \rho_v)]^{0.25}}. \quad (12)$$

The RCA model shows that number of turns (N) and FR do not significantly predict the value of thermal resistance of a PHP. The orientation of a PHP (θ) is found to be less significant compared with other input variables as shown in figure 6. Hence, other input variables such as length of the condenser section (L_c), length of the evaporator section (L_e), input heat (Q), working fluid (WF), outer diameter (D_o) and inner diameter (D_i) can be grouped and represented as per Eq. (13):

$$Ku = f(Bo, Mo, \Pr, Ja, D_o/D_i, L_c/L_e, D_i/L_e). \quad (13)$$

The dimensionless number D_o/D_i represents the geometrical characteristics of the wall. $D_i/L_e$and L_c/L_e are ratios of the inner diameter to the evaporator length and evaporator length to condenser length, respectively, representing the aspect ratio and geometrical characteristics of PHP. Other dimensionless numbers defined are Bond number (Bo), Morton number (Mo), Prandtl number of liquid (Pr) and Jakob number (Ja) through Eqs. (14)–(17):

$$\text{Bond number Bo} = \sqrt{\frac{g(\rho_l - \rho_v)D^2}{\sigma}}, \quad (14)$$

$$\text{Morton number } Mo = \frac{\mu[g(\rho_l - \rho_v)]^{0.25}}{\rho_v^{0.5}\sigma^{0.75}}, \quad (15)$$

$$\text{Prandtl number } p_r = \frac{\mu c_p}{k}, \quad (16)$$

$$\text{Jakob number } Ja = \frac{C_p \Delta T}{h_{lv}}. \quad (17)$$

The dimensionless numbers depend on thermophysical properties of the WFs, which in turn depend on temperature. Temperature data reported in the literature are very limited [41–48]. Hence, the subsequent development of correlation is carried out with a total of 920 data. The thermophysical properties of WFs are calculated based on the average temperature [(Te + Tc)/2] of the PHP. In order to develop the linear correlation for Ku as a function of aforementioned dimensionless parameters (Pr, Ja, Bo, Mo, L_e/L_c, D_o/D_i and D_i/L_e), the backward regression analysis is carried out as discussed before. All the dimensionless numbers are found to be significant (p-value is less than 0.05 for all) as shown in table 8. The linear correlation developed for Ku is shown as Eq. (18). The prediction accuracy of Eq. (18) is observed to be good with R^2 as 0.9483 and Adjusted R^2 as 0.9479.

$$K_u = -0.0713 - 0.0028P_r + 0.2535J_a + 0.0115B_o - 0.2651\frac{D_i}{L_e} + 0.0044\frac{L_c}{L_e} + 0.0278\frac{D_o}{D_i} - 0.09M_o. \quad (18)$$

Table 8. Result summary of backward regression analysis for linear regression.

Model no.		Intercept	Pr	Ja	Bo	D_i/L_e	L_c/L_e	D_o/D_i	Mo
01	Coefficients	−0.0713	−0.0028	0.2535	0.0115	−0.2651	0.0044	0.0278	0.0900
	t-stat	−7.6987	−6.1215	78.0978	3.6731	−10.566	18.6046	6.6315	4.8176
	p value	0.0000	0.0000	0.0000	0.0003	0.0000	0.0000	0.0000	0.0000
		R^2 = 0.9483, Adjusted R^2 = 0.9479							

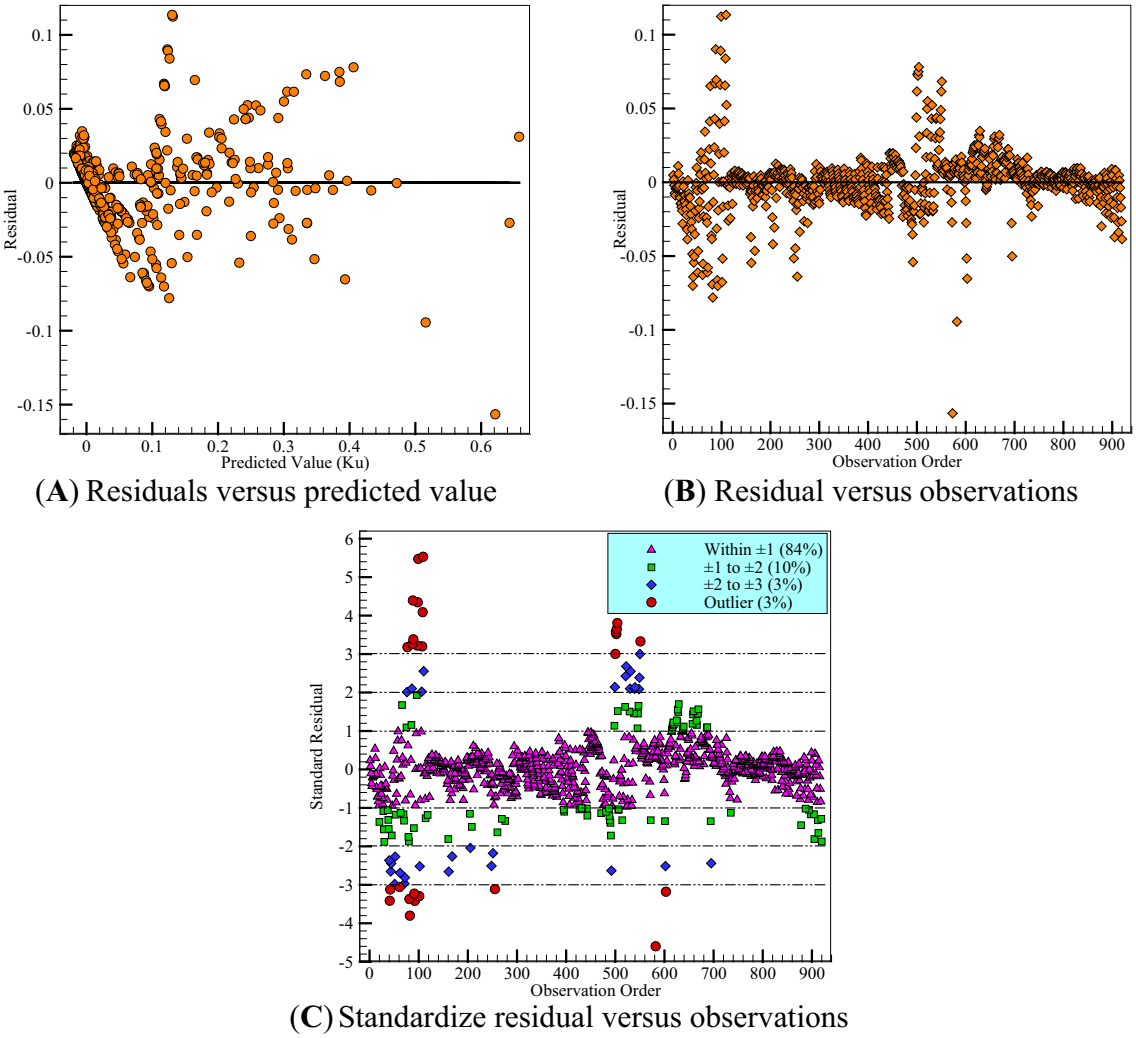

Figure 7. Residual plots for linear regression model (Eq. (18)).

Table 9. Result summary of backward regression analysis for power-law regression.

Model no.		Intercept	ln(*Mo*)	ln(D_i/L_e)	ln(*Ja*)	ln(*Pr*)	ln(D_o/D_i)	ln(L_c/L_e)	ln(*Bo*)
01	Coefficients	−7.9620	−1.2046	1.0629	0.5006	1.1771	2.0418	0.1469	**0.3232**
	t Stat	−19.8467	−14.4964	14.3788	10.9505	9.4756	7.2744	2.2984	**1.6823**
	p-value	0.0000	0.0000	0.0000	0.0000	0.0000	0.0000	0.0218	**0.0929**
				R^2 = 0.9035, Adjusted R^2 = 0.9028					
02	Coefficients	−8.1449	−1.3136	1.1136	0.5044	1.3509	1.8101	**0.0906**	*
	t Stat	−21.0706	−25.2037	16.4889	11.0362	19.5789	7.3939	**1.6621**	*
	p-value	0.0000	0.0000	0.0000	0.0000	0.0000	0.0000	**0.0968**	*
				R^2 = 0.9032, Adjusted R^2 = 0.9026					
03	Coefficients	−7.7124	−1.3050	1.2021	0.5310	1.3648	1.7758	*	*
	t Stat	−26.9575	−25.1385	28.8883	12.3955	19.9063	7.2727	*	*
	p-value	0.0000	0.0000	0.0000	0.0000	0.0000	0.0000	*	*
				R^2 = 0.9029, Adjusted R^2 = 0.9024					

It is worth noting that for a linear regression model, the residual tests are very important to check the goodness of fit for the developed model. The residual plots for linear regression model of Eq. (18) have been shown in figure 7. Figure 7A shows the distribution of residuals as a function of predicted values of *Ku*. The distribution is observed to be

random and does not show any significant pattern or trend. This means that the residuals do not contain any predictive information. This shows that the model is correct for all fitted (predicted) values of *Ku*. Another essential condition of a linear regression model is that the error terms should be independent, which can be seen by plotting residuals against observation order as shown in figure 7B. The residuals bounce randomly around the zero line throughout the range of observation as it would be expected. In general, residuals exhibiting normal random noise around the zero line suggests that there is no serial correlation. Moreover, standardized residual (residual/standard deviation of residual) versus observation graph is plotted to detect the outliers as shown in figure 7C. Approximately 68% standardized residuals fall within ±1 limit, 95% within ±2 and all of them fall between ±3 limit.

Table 10. Validity ranges of parameters used for linear (Eq. (18)) and power-law (Eq. (21)) regression modelling.

Parameters	Pr	Ja	D_i/L_e	D_o/D_i	Mo	L_c/L_e	Bo
Range	1–14	0–2.5	0–0.25	1.5–2	0–0.36	0.5–30	0.5–3

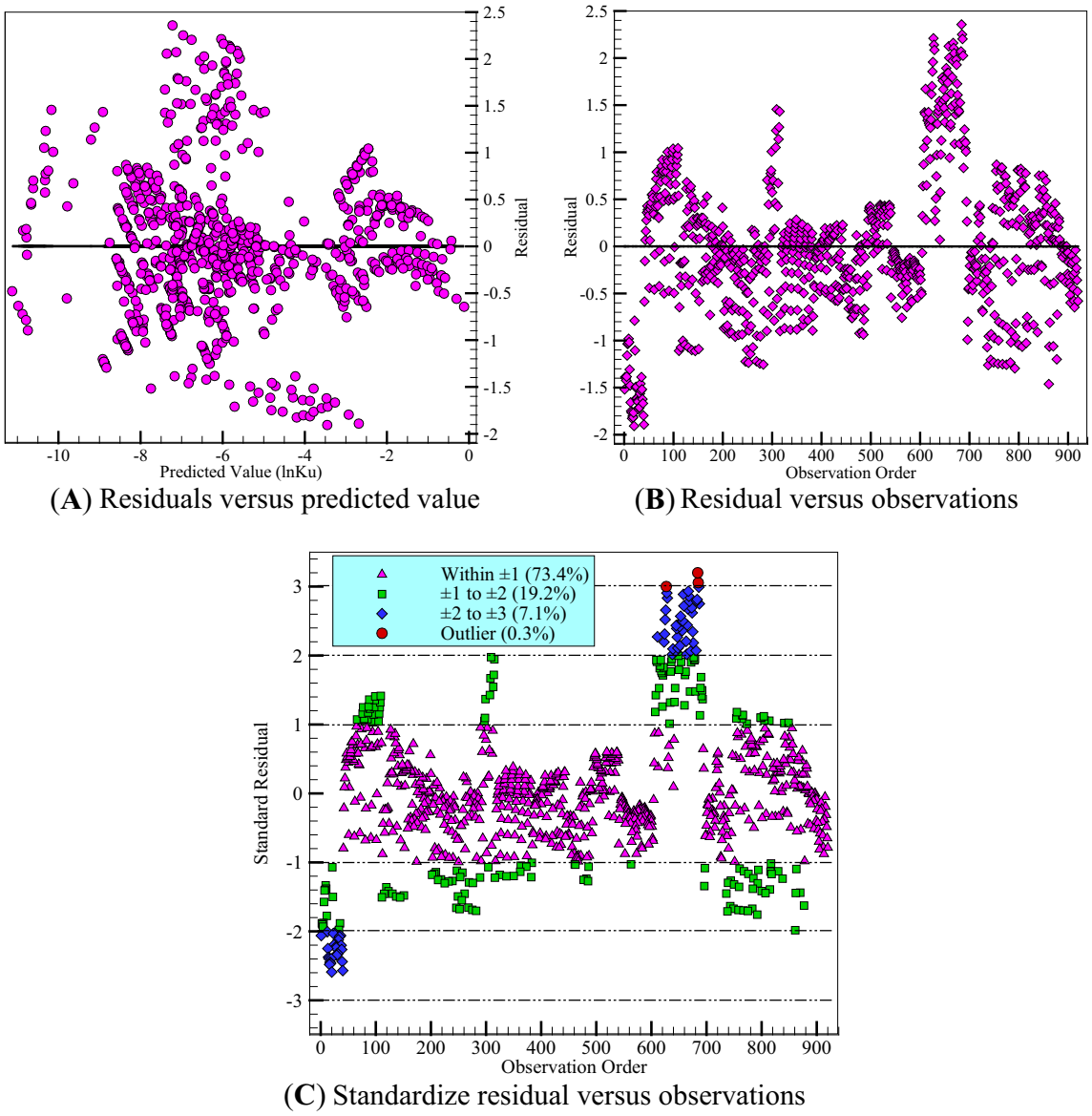

Figure 8. Residual plots for power regression model (Eq. (21)).

Standardized residuals observed outside ±3 limit are considered as outliers. It is seen that 84% data are observed between the limit ±1, 94% between the ±2 and 97% are within the limit ±3. Only 3% data (outlier) fall outside the range, which shows the goodness of fit for Eq. (18).

Most of the *Ku* correlations reported in the literature [57–63] are in the form of the power law and hence it is also developed in the present paper. Power-law regression model for *Ku* is given by Eq. (19). It is converted into equivalent linear form by taking natural log on both sides and shown as Eq. (20).

$$Ku = \alpha P_r^a J_a^b B_o^c \left(\frac{D_i}{L_e}\right)^d \left(\frac{L_c}{L_e}\right)^e \left(\frac{D_0}{D_i}\right)^f M_0^g, \tag{19}$$

$$\ln(Ku) = \ln\alpha + a\ln(P_r) + b\ln(J_a) + c\ln(B_o) + d\ln\left(\frac{D_i}{L_e}\right) + e\ln\left(\frac{L_c}{L_e}\right) + f\ln\left(\frac{D_0}{D_i}\right) + g\ln(M_0), \tag{20}$$

$$Ku = 0.0004 P_r^{1.3648} J_a^{0.5310} \left(\frac{D_i}{L_e}\right)^{1.2021} \left(\frac{D_0}{D_i}\right)^{1.7758} M_0^{-1.3050} \tag{21}$$

All dimensionless data (x) are transformed into natural log form ($\ln x$) and then backward regression analysis is carried out for Eq. (20). The power-law correlation

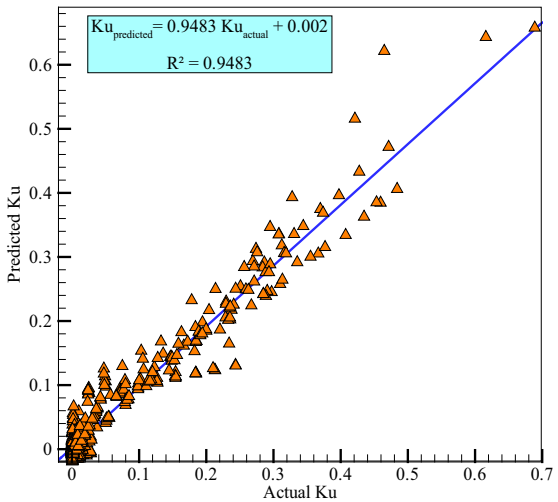

(**A**) Linear correlation (Eq. (18)).

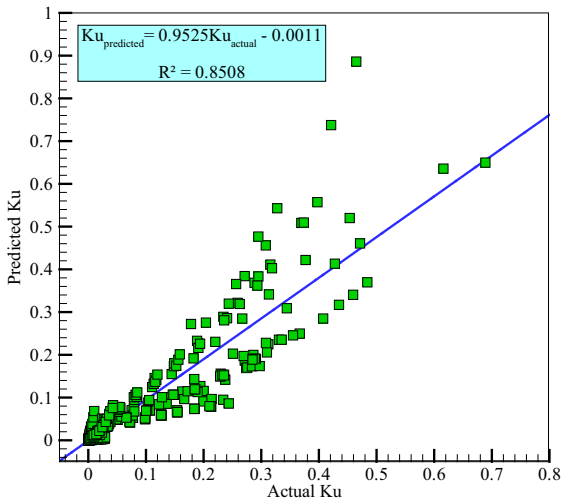

(**B**) Power-law correlation (Eq. (21))

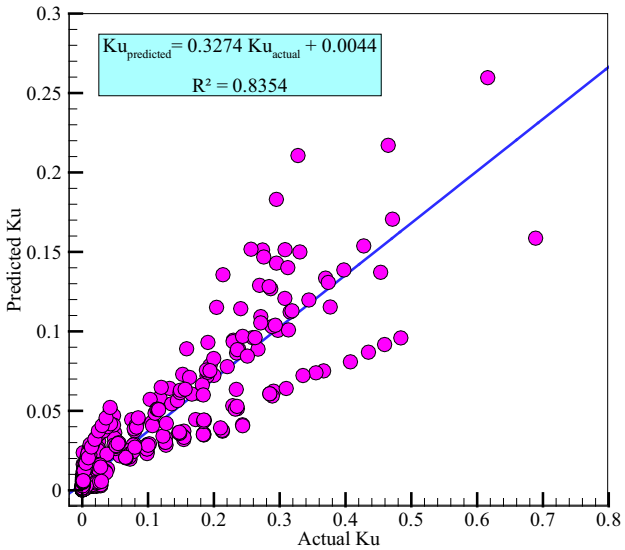

(**C**) Power-law correlation proposed by Shafii *et al* (Eq. (22)).

Figure 9. Comparison between predicted *Ku* and actual *Ku* for a total of 920 data.

developed for *Ku* is represented by Eq. (21) and analogous regression results are shown in table 9. The values of R^2 (0.9029) and Adjusted R^2 (0.9024) are not observed to be affected by the reduction of input parameters. It eliminates two parameters of Bond number and the ratio L_c/L_e from the correlation as compared with linear regression correlation (Eq. (18)). Hence, the prediction accuracy of the power-law regression model is observed to be poor as compared with the linear regression model. Validity ranges of the parameter used for linear (Eq. (18)) and power-law (Eq. (21)) regression modelling are tabulated in table 10. As discussed before for a linear regression model, similar residual tests are carried out to verify the goodness of fit for the developed power-law regression model and shown in figure 8.

$$Ku = a\left(\frac{C_p\Delta T}{h_{lv}}\right)^{b}\left(\frac{\mu c_p}{k}\right)^{-0.7}\left(D_i\sqrt{\frac{g(\rho_l-\rho_v)}{\sigma}}\right)^{0.85}\left(\frac{\mu(g\Delta\rho)^{0.25}}{\rho_v^{0.5}\sigma^{0.75}}\right)^{0.8}\left(\frac{D_i}{L_e}\right)^{0.7}\left(\frac{D_o}{D_i}\right)^{2.6} \tag{22}$$

where $a = -1258(FR)^4+2663.1(FR)^3-2028.9(FR)^2 + 655.28(FR) - 71.22 \quad b = -142.5(FR)^4 + 301.5(FR)^3-227.6(FR)^2+72.21(FR) - 6.87$

The prediction accuracy of the developed linear and power-law regression correlations is compared with two datasets as shown in figures 9 and 10. In addition to this, the correlation proposed by Shafii *et al* [29] as Eq. (22)

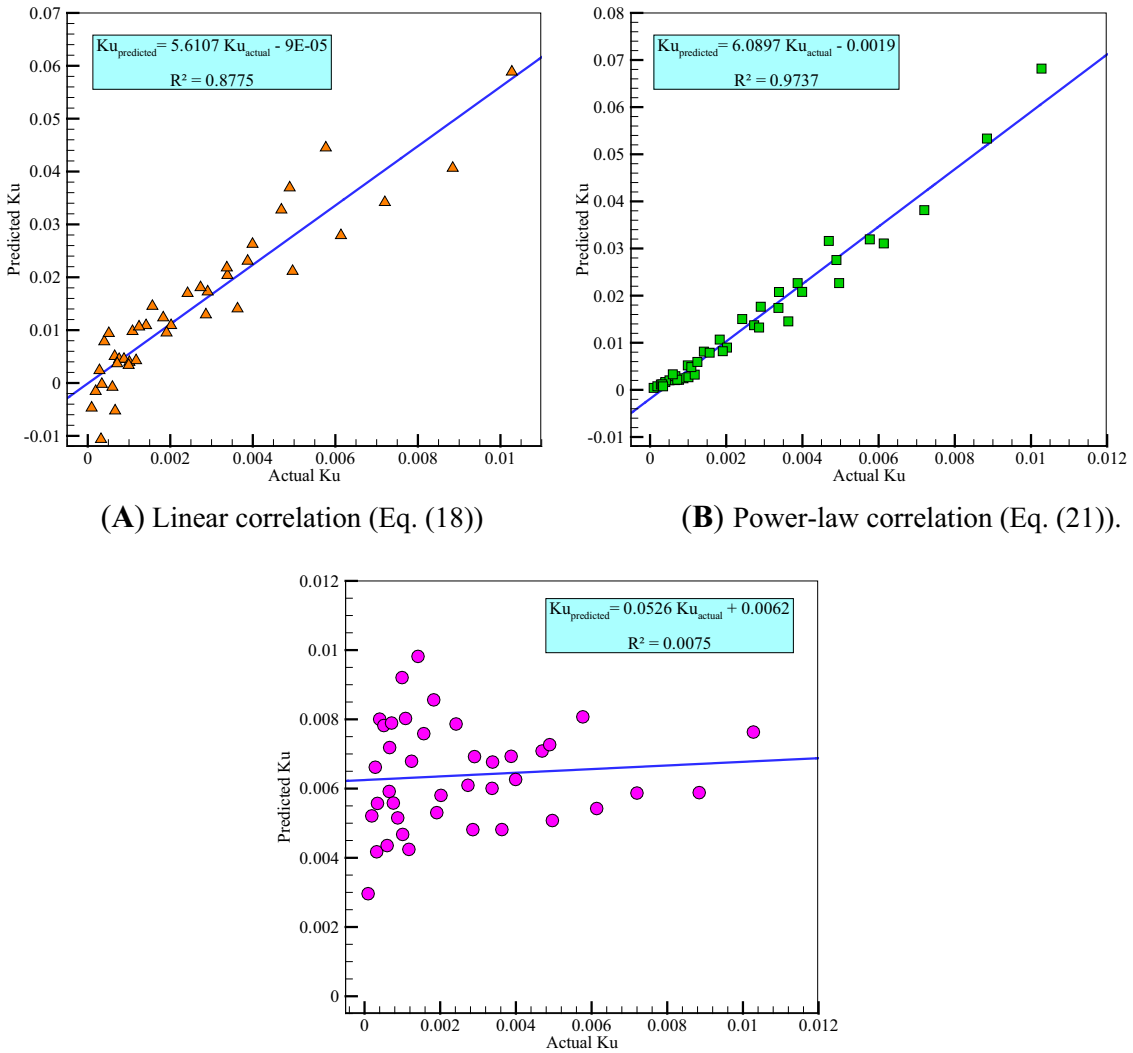

(**A**) Linear correlation (Eq. (18))

(**B**) Power-law correlation (Eq. (21)).

(**C**) Power-law correlation proposed by Shafii *et al* (Eq. (22)).

Figure 10. Comparison between predicted *Ku* and actual *Ku* based on authors' data [4].

developed on the accessible dataset in the literature is also compared with these datasets. Figure 9 shows the comparison between predicted *Ku* and actual *Ku* based on total 920 data. Figure 10 shows the comparison between predicted *Ku* and actual *Ku* based on the authors' experimental data [4]. It is observed from figures 9 and 10 that linear correlation prediction is better for overall dataset while power-law correlation prediction is better for a specific dataset of authors' experiments. In both the comparisons, the prediction accuracy of Eq. (22) is found to be poor as compared with developed correlations (Eqs. (18)–(21)). The poor agreement may be due to authors' wide dataset used for the development of Eqs. (18)–(21) as compared with Eq. (22) of Shafii *et al* [29].

4. Conclusion

The present research work is an effort towards the development of thermal performance prediction models of a PHP based on ANN and RCA approach using literature-based dataset. The authors have for the first time involved totally nine influencing parameters and a wide range of dataset (1652) for the development of prediction models in a systematic way. Thermal resistance is considered as a performance parameter. The first prediction model is developed based on feed-forward back-propagation neural network and found to be in overall agreement with higher prediction accuracy (R^2=0.89). In the absence of a significant relationship between output and input parameters through ANN model, the second prediction model is developed using RCA approach. The backward regression analysis is carried out to develop the correlation. RCA model is not observed to be in agreement (R^2 = 0.38) for the prediction of thermal resistance using dimensional parameters (D_i, D_o, *Le*, *Lc*, *N*, *WF*, θ, *FR*, *Q*). Hence, the third model is developed for the prediction of thermal performance based on dimensionless Kutateladze (*Ku*) number as a function of Jacob number, Morton number, Bond number and Prandtl number and dimensionless geometrical characteristics of a PHP. Linear and power-law regression models are developed. The prediction accuracy of the linear model is observed to be in overall agreement (R^2 = 0.95) as compared with power-law correlation and Shafii *et al* [29] correlation. The present research can be helpful to design and optimize the influencing parameters of a PHP for practical applications such as electronics, automobile radiator and fuel cell cooling.

Funding The funding was provided by SVNIT, Surat (Grant No. Dean(R&C)/1503/2013-14).

Nomenclature

Ku	Kutateladze number
Ja	Jakob number
Mo	Morton number
Bo	bond number
Pr	Prandtl number
R_{th}	thermal resistance (K/W)
Y_p	predicted output by the regression model
h_{lv}	latent heat of vaporization (J/kg)
C_p	specific heat at constant pressure (J/kg K)
R^2	coefficient of determination
R^2_{adj}	adjusted coefficient of determination
D	diameter (mm)
L	length (mm)
K	thermal conductivity (W/m K)
N	number of turns
Q	heat input (W)
Y	real output
X	input parameter
A	coefficient
T	temperature
R	coefficient of correlation
x	input data
w	weight
b	bias
g	gravitational acceleration (m/s^2)
e	error
N	number of observations
K	number of predictors

Abbreviations

FR	filling ratio
WF	working fluid
ANN	artificial neural network
RCA	regression/correlation analysis
Purelin	linear transfer function
tansig	tangent sigmoid function
logsig	log-sigmoid transfer function
RBF	radial basis function
MSE	mean square error
SSE	sum squared error
SST	sum squared total
t-stat	*t*-statistic
MARD	mean absolute relative deviation

Greek symbols

μ	viscosity (Pa s)
ρ	density (kg/m^3)
σ	surface tension (N/m)
θ	orientation

Subscripts

l	liquid
e	evaporator
c	condenser
i	inner
o	outer
v	vapour

References

[1] Akachi H 1990 *Structure of a heat pipe*. Patent No. 4921041

[2] Groll M and Khandekar S 2003 Pulsating heat pipes: progress and prospects. In: *Proceedings of the International Conference on Energy and the Environment*, China

[3] Han X, Wang X, Zheng H, Xu X and Chen G 2016 Review of the development of pulsating heat pipe for heat dissipation. *Renewable and Sustainable Energy Reviews* 59: 692–709

[4] Patel V M, Gaurav and Mehta H B 2017 Influence of working fluids on startup mechanism and thermal performance of a closed loop pulsating heat pipe. *Applied Thermal Engineering* 110: 1568–1577

[5] Zhang Y W, Faghri A and Shafii M B 2002 Analysis of liquid–vapor pulsating flow in a U-shaped miniature tube. *International Journal of Heat and Mass Transfer* 45: 2501–2508

[6] Zhang Y W and Faghri A 2003 Oscillatory flow in pulsating heat pipes with arbitrary numbers of turns. *Journal of Thermophysica and Heat and Transfer* 17: 340–347

[7] Yuan D Z, Qu W and Ma T Z 2010 Flow and heat transfer of liquid plug and neighbouring vapor slugs in a pulsating heat pipe. *International Journal of Heat and Mass Transfer* 53: 1260–1268

[8] Ma H B, Borgmeyer B, Cheng P and Zhang Y 2008 Heat transport capability in an oscillating heat pipe. *Journal of Heat Transfer – Transactions of the ASME* 130, https://doi.org/10.1115/1.2909081

[9] Kim S J, Zhang Y W and Choi J 2013 Effects of fluctuations of heating and cooling section temperatures on the performance of a pulsating heat pipe. *Applied Thermal Engineering* 58: 42–51

[10] Shao W and Zhang Y W 2011 Effects of film evaporation and condensation on oscillatory flow and heat transfer in an oscillating heat pipe. *Journal of Heat Transfer – Transactions of the ASME* 133: 042901

[11] Dilawar M and Pattamatta A 2013 A parametric study of oscillatory two-phase flows in a single turn pulsating heat pipe using a non-isothermal vapor model. *Applied Thermal Engineering* 51: 1328–1338

[12] Sakulchangsatjatai P, Terdtoon P, Wongratanaphisan T, Kamonpet P and Murakami M 2004 Operation modeling of closed-end and closed-loop oscillating heat pipes at normal operating condition. *Applied Thermal Engineering* 24: 995–1008

[13] Mameli M, Marengo M and Zinna S 2012 A numerical model of a multi-turn closed loop pulsating heat pipe: effects of the local pressure losses due to meanderings. *International Journal of Heat and Mass Transfer* 55: 1036–1047

[14] Qu J, Wu H Y, Cheng P and Wang X 2009 Nonlinear analyses of temperature oscillations in a closed loop pulsating heat pipe. *International Journal of Heat and Mass Transfer* 52(15–16): 3481–3489

[15] Song Y X and Xu J L 2009 Chaotic behavior of pulsating heat pipes. *International Journal of Heat and Mass Transfer* 52: 2932–2941

[16] Qu W and Ma H B 2007 Theoretical analysis of start-up of a pulsating heat pipe. *International Journal of Heat and Mass Transfer* 50: 2309–2316

[17] Wang J, Ma He and Zhu Q 2015 Effects of the evaporator and condenser length on the performance of pulsating heat pipes. *Applied Thermal Engineering* 91: 1018–1025

[18] Pouryoussefi S M and Zhang Y 2016 Numerical investigation of chaotic flow in a 2D closed loop pulsating heat pipe. *Applied Thermal Engineering* 98: 617–627

[19] Jokar A, Godarzi A A, Saber M and Shafii M B 2016 Simulation and optimization of a pulsating heat pipe using the artificial neural network and genetic algorithm. *Heat and Mass Transfer*

[20] Khandekar S, Cui X and Groll M 2002 Thermal performance modeling of pulsating heat pipes by artificial neural network. In: *Proceedings of the 12th International Heat Pipe Conference*, pp. 215–219

[21] Shokouhmand H, Gharib N and Bahrami H 2006 Modeling of closed loop pulsating heat pipes by neural networks. In: *Proceedings of the 8th Biennial ASME Conference on Engineering Systems Design and Analysis*, Torino, Italy, ESDA2006-95417

[22] Patel V M and Mehta H B 2016 Artificial neural network modeling of a closed loop pulsating heat pipe. *World Academy of Science, Engineering, and Technology -International Journal of Mechanical, Aerospace, Industrial, Mechatronics, and Manufacturing Engineering* 10: 1754–1757

[23] Jia Qiang E, Yu Qiang L and Jin ke G 2011 Function chain neural network prediction on heat transfer performance of oscillating heat pipe based on the grey relational analysis. https://doi.org/10.1007/s11771-011-0895

[24] Chien K H, Lin Y T, Chen Y R, Yang K S and Wang C C 2012 A novel design of pulsating heat pipe with fewer turns applicable to all orientations. *International Journal of Heat and Mass Transfer* 55: 5722–5728, https://doi.org/10.1016/j.ijheatmasstransfer.2012.05.068

[25] Karthikeyan V K, Ramachandran K, Pillai B C and Brusly Solomon A 2014 Effect of nanofluids on thermal performance of closed loop pulsating heat pipe. *Experimental Thermal and Fluid Science* 54: 171–178, https://doi.org/10.1016/j.expthermflusci.2014.02.007

[26] Lin Y H, Kang S W and Chen H L 2008 Effect of silver nano-fluid on pulsating heat pipe thermal performance. *Applied Thermal Engineering* 28: 1312–1317

[27] Baitule D A 2013 Experimental analysis of closed loop pulsating heat pipe with variable filling. *International Journal of Mechanical Engineering and Robotics Research* 2

[28] Clement J and Wang X 2013 Experimental investigation of pulsating heat pipe performance with regard to the fuel cell cooling application. *Applied Thermal Engineering* 50: 268–274, https://doi.org/10.1016/j.applthermaleng.2012.06.017

[29] Shafii M B, Arabnejad S, Saboohi Y and Jamshidi H 2010 Experimental investigation of pulsating heat pipes and a proposed correlation. *Heat Transfer Engineering* 31: 854–861, https://doi.org/10.1080/01457630903547636

[30] Verma B, Yadav V L and Srivastava K K 2013 Experimental studies on thermal performance of a pulsating heat pipe with methanol/DI water. *Journal of Electronics Cooling and Thermal Control* 3: 27–34

[31] Naik R, Varadarajan V, Pundarika G and Narasimha K R 2013 Experimental investigation and performance evaluation

of a closed loop pulsating heat pipe. *Journal of Applied Fluid Mechanics* 6: 267–275.

[32] Tseng C Y, Yang K S, Chien K H, Jeng M S and Wang C C 2014 Investigation of the performance of pulsating heat pipe subject to uniform/alternating tube diameters. *Experimental Thermal and Fluid Science* 54: 85–92, https://doi.org/10.1016/j.expthermflusci.2014.01.019

[33] Ji Y, Ma H, Su F and Wang G 2011 Particle size effect on heat transfer performance in an oscillating heat pipe. *Experimental Thermal and Fluid Science* 35: 724–727, https://doi.org/10.1016/j.expthermflusci.2011.01.007

[34] Kothare P C B, Raizada P K S and Chavhan B K 2015 Thermal performance of closed loops pulsating heat pipe at various dimension and heat input. *International Research Journal of Engineering and Technology* 2(7): 739–744

[35] Pachghare P R and Mahalle A M 2014 Thermo-hydrodynamics of closed loop pulsating heat pipe: an experimental study. *Journal of Mechanical Science and Technology* 28: 3387–3394, https://doi.org/10.1007/s12206-014-0751-9

[36] Han H, Cui X, Zhu Y, Xu T, Sui Y and Sun S 2016 Experimental study on a closed-loop pulsating heat pipe charged with water-based binary zeotropes and the corresponding pure fluids. *Energy* 109: 724–736, https://doi.org/10.1016/j.energy.2016.05.061

[37] Wang S, Lin Z, Zhang W and Chen J 2009 Experimental study on pulsating heat pipe with functional thermal fluids. *International Journal of Heat and Mass Transfer* 52: 5276–5279, https://doi.org/10.1016/j.ijheatmasstransfer.2009.04.033

[38] Mohammadi M, Mohammadi M, Ghahremani A R, Shafii M B and Mohammadi N 2014 Experimental investigation of thermal resistance of a ferrofluidic closed-loop pulsating heat pipe. *Heat Transfer Engineering* 35: 25–33, https://doi.org/10.1080/01457632.2013.810086

[39] Y Wang 2015 Experimental investigations on operating characteristics of a closed loop pulsating heat pipe. *Frontiers in Energy*. 9: 134–141.

[40] Mameli M, Manno V, Filippeschi S and Marengo M 2014 Thermal instability of a closed loop pulsating heat pipe: combined effect of orientation and filling ratio. *Experimental Thermal and Fluid Science* 59: 222–229, https://doi.org/10.1016/j.expthermflusci.2014.04.009

[41] Cui X, Zhu Y, Li Z and Shun S 2014 A combination study of operating characteristics and heat transfer mechanism for pulsating heat pipe. *Applied Thermal Engineering* 65: 394–402, https://doi.org/10.1016/j.applthermaleng.2014.01.030

[42] P R Pachghare and A M Mahalle 2012 Effect of pure and binary fluids on closed loop pulsating heat pipe thermal performance. *Procedia Engineering* 51: 624–629 (NUiCONE)

[43] Borkar R S and Pachghare P R 2015 Effect of working fluid, filling ratio and number of turns on pulsating heat pipe thermal performance. *Frontiers in Heat Pipes*. https://doi.org/10.5098/fhp.6.4

[44] Yang H, Khandekar S and Groll M 2008 Operational limit of closed loop pulsating heat pipes. *Applied Thermal Engineering*. 28: 49–59, https://doi.org/10.1016/j.applthermaleng.2007.01.033

[45] Khandekar S, Dollinger N and Groll M 2003 Understanding operational regimes of closed loop pulsating heat pipes: an experimental study. *Applied Thermal Engineering* 23: 707–719, https://doi.org/10.1016/S1359-4311(02)00237-5

[46] Akter Jahan S, Ali M and Quamrul Islam M 2013 Effect of inclination angles on heat transfer characteristics of a closed loop pulsating heat pipe. *Procedia Engineering*. *56*: 82–87, https://doi.org/10.1016/j.proeng.2013.03.092

[47] Han H, Cui X, Zhu Y and Sun S 2014 A comparative study of the behaviour of working fluids and their properties on the performance of pulsating heat pipes. *International Journal of Thermal Sciences* 82: 138–147, https://doi.org/10.1016/j.ijthermalsci.2014.04.003

[48] Mameli M, Manno V, Filippeschi S and Marengo M 2014 Thermal instability of a closed loop pulsating heat pipe: combined effect of orientation and filling ratio. *Experimental Thermal and Fluid Science* 59: 222–229, https://doi.org/10.1016/j.expthermflusci.2014.04.009

[49] G Notton, C Paoli and S Diaf 2013 Estimation of tilted solar irradiation using artificial neural networks. *Energy Proceedia* 42: 33–42, https://doi.org/10.1016/j.egypro.2013.11.003

[50] L Thiaw, G Sow and S Fall 2014 Application of neural networks techniques in renewable energy systems. In: *Proceedings of the First International Conference on Systems Informatics, Modelling and Simulation*, IEEE

[51] Alam S, Kaushik S C and Garg S N 2009 Assessment of diffuse solar energy under general sky condition using the artificial neural network. *Applied Energy* 86: 554–564

[52] Ertunc H M and Hosoz M 2006 Artificial neural network analysis of a refrigeration system with an evaporative condenser. *Applied Thermal Engineering* 26: 627–635, https://doi.org/10.1016/j.applthermaleng.2005.06.002

[53] Huang C, Bensoussan A, Edesess M and Tsui K L 2016 Improvement in the artificial neural network-based estimation of grid-connected photovoltaic power output. *Renewable Energy* 97: 838–848, https://doi.org/10.1016/j.renene.2016.06.043

[54] Kshirsagar C M and Anand R 2017 Artificial neural network applied forecast on a parametric study of Calophyllum inophyllum methyl ester–diesel engine out responses. *Applied Energy* 189: 555–567, https://doi.org/10.1016/j.apenergy.2016.12.045

[55] Sayin C, Ertunc H M, Hosoz M, Kilicaslan I and Canakci M 2007 Performance and exhaust emissions of a gasoline engine using the artificial neural network. *Applied Thermal Engineering* 27: 46–54, https://doi.org/10.1016/j.applthermaleng.2006.05.016

[56] Sözen A, Arcaklioğlu E and Özalp M 2003 A new approach to the thermodynamic analysis of ejector–absorption cycle: artificial neural networks. *Applied Thermal Engineering* 23: 937–952, https://doi.org/10.1016/S1359-4311(03)00034-6

[57] Arslan G and Özdemir M 2008 Correlation to predict heat transfer of an oscillating loop heat pipe consisting of three interconnected columns. *Energy Conversion and Management* 49: 2337–2344, https://doi.org/10.1016/j.enconman.2008.01.014

[58] Goshayeshi H R, Izadi F and Bashirnezhad K 2017 Comparison of heat transfer performance on closed pulsating heat pipe for Fe_3O_4 and γFe_2O_3 for achieving an empirical correlation. *Physica E: Low-Dimensional Systems and Nanostructures* 89: 43–49, https://doi.org/10.1016/j.physe.2017.01.014

[59] Kammuang L N, Hudakorn T and Terdtoon P 2010 Establishment, verification, and application of a correlation to predict the maximum heat flux of a horizontal closed-loop pulsating heat pipe. *Energy Research Journal* 1: 96–103, https://doi.org/10.3844/erjsp.2010.96.103

[60] Kammuang-lue N, Onai K, Sakulchangsatjatai P and Terdtoon P 2014 Correlation to predict thermal performance according to working fluids of vertical closed-loop pulsating heat pipe. *International Journal of Mechanical, Aerospace, Industrial, Mechatronics and Manufacturing Engineering* 8: 949–957

[61] Katpradit T, Wongratanaphisan T, Terdtoon P, Kamonpet P, Polchai A and Akbarzadeh A 2005 Correlation to predict heat transfer characteristics of a closed-end oscillating heat pipe at a critical state. *Applied Thermal Engineering* 25: 2138–2151, https://doi.org/10.1016/j.applthermaleng.2005.01.009

[62] Khandekar S, Charoensawan P, Groll M and Terdtoon P 2003 Closed loop pulsating heat pipes – part B: visualization and semi-empirical modeling. *Applied Thermal Engineering* 23: 2021–2033, https://doi.org/10.1016/S1359-4311(03)00168-6

[63] Waowaew N, Terdtoon P, Maezawa S, Kamonpet P and Klongpanich W 2003 Correlation to predict heat transfer characteristics of a radially rotating heat pipe at the vertical position. *Applied Thermal Engineering* 23: 1019–1032, https://doi.org/10.1016/S1359-4311(03)00028-0